Non-linear bioconvection in a deep suspension of gyrotactic swimming micro-organisms

M. A. Bees[1] and N. A. Hill[2]

Department of Applied Mathematics,

University of Leeds, Leeds LS2 9JT, U.K.

Page heading: Non-linear deep bioconvection

Key words: bioconvection patterns, swimming micro-organisms, gyrotaxis, travelling waves, Fokker-Planck equation, amplitude equation

[1]Present address: Physics Department, Building 309, Danish Technical University, DK-2800 Lyngby, Denmark. (*e–mail:* Martin.A.Bees@fysik.dtu.dk)

[2]Author to whom reprint requests should be addressed. (*e–mail:* N.A.Hill@Leeds.ac.uk)

August 3, 1998

The non-linear structure of deep, stochastic, gyrotactic bioconvection is explored. A linear analysis is reviewed and a weakly non-linear analysis justifies its application by revealing the supercritical nature of the bifurcation. An asymptotic expansion is used to derive systems of partial differential equations for long plume structures which vary slowly with depth. Steady state and travelling wave solutions are found for the first order system of partial differential equations and the second order system is manipulated to calculate the speed of vertically travelling pulses. Implications of the results and possibilities of experimental validation are discussed.

1 Introduction

Bioconvection is a term used to describe the bulk fluid motion and cell aggregation patterns due to freely swimming micro-organisms in suspension. For a comprehensive review of the subject and related fields, see Pedley & Kessler (1992). There are a number of mechanical processes involved that bias the micro-organisms to swim in preferred directions. One such mechanism is the tendency of the micro-organisms to swim upwards due to their asymmetric mass distribution. If there is an upper boundary and the cells have greater density than the fluid in which they swim, then a Rayleigh-Bénard or overturning type of instability can arise, whenever the cells aggregate near the upper boundary so that a layer of dense fluid overlays less dense fluid. Additionally, straining fields and vorticity in the fluid can influence the average local cell-swimming direction, causing the cells to swim towards regions of downwelling fluid. This mechanism is known as gyrotaxis, after Kessler (1984). Again, if the material density of the cells is greater than the density of the fluid, then an aggregation of cells will cause the fluid to sink faster in that region, thus attracting more cells. This instability is called a gyrotactic instability. Some examples of bioconvection patterns in shallow suspensions of the alga *Chlamydomonas nivalis* can be found in Bees (1996) and Bees & Hill (1997). *C. nivalis* exhibits both forms of instability mentioned above. Childress *et al.* (1975) developed a model to describe the Rayleigh-Bénard type instability for purely upswimming cells and this was later extended by Pedley *et al.* (1988), Hill *et al.* (1989), Pedley & Kessler (1990), Bees (1996) and Bees & Hill (1998b) to include the gyrotactic instability in either deterministic

or stochastic formulations. For deep suspensions without an upper boundary, purely upswimming models (Childress *et al.* 1975) are not unstable (cannot produce patterns) unlike models incorporating gyrotaxis. In experiments with deep suspensions of *C. nivalis*, long plume structures form in the interior of the suspension and are not initiated at the boundaries, confirming that *C. nivalis* is gyrotactic (Kessler 1985a). Experiments also show evidence of vertically travelling pulses that move down the plumes (see Kessler 1985b). Observations indicate that larger pulses travel faster than smaller pulses. The larger pulses can catch the smaller pulses, whereupon they merge.

In this paper, we consider the fully non-linear equations for a deep suspension as proposed by Pedley & Kessler (1990). In particular, we employ the solutions obtained by Bees *et al.* (1998b) from a spherical harmonic expansion of the Fokker-Planck equation that describes the stochastic orientation of swimming micro-organisms subject to gravitational and viscous torques.

Initially, in Section 3, we explore the linear analysis considered by Pedley *et al.* (1988), which highlights the scalings required for the weakly non-linear analysis of Section 5. Then, in order to simplify the equations, Section 4 considers the experimentally realizable case of long vertical wavelength patterns in deep suspensions. This provides a set of non-linear partial differential equations, the first pair of which involve the vertical coordinate, z, in a passive manner. A weakly non-linear analysis of deep bioconvection for long vertical wavelengths is considered in Section 5 in order to characterize the bifurcation to instability, and thus determine if the linear analysis can be used to predict the initial pattern wavelengths. In Section 6 we consider the horizontal steady state solutions for long vertical wavelengths by numerically integrating the equations and, in Section 7, time dependence is included in the form of horizontally-travelling vertical plumes subject to a small forcing flow field. Section 8 derives an equation for variations in the z-direction and calculates the wavespeed of small amplitude vertically-travelling pulses. The generalization of the above methods to three-dimensional fluid flows is considered in Section 9. In the Discussion, we summarize our results from both mathematical and biological perspectives.

2 Governing Equations

We begin by stating the main equations governing the flow and concentration fields in an infinite domain (as proposed by Pedley & Kessler 1990):

$$\nabla \cdot \mathbf{u} = 0, \tag{1}$$

$$\rho \left(\frac{\partial \mathbf{u}}{\partial t} + \mathbf{u} \cdot \nabla \mathbf{u} \right) = -\nabla p_e + nv\Delta\rho\mathbf{g} + \mu\nabla^2\mathbf{u} \tag{2}$$

and

$$\frac{\partial n}{\partial t} = -\nabla \cdot \left[n \left(\mathbf{u} + V_s \langle \mathbf{p} \rangle \right) - \mathbf{D} \cdot \nabla n \right], \tag{3}$$

where $\mathbf{u}(\mathbf{x})$ is the fluid velocity, $\langle \mathbf{p}(\mathbf{x}) \rangle$ is the mean cell swimming direction, V_s is the mean cell swimming speed, $\mathbf{D}(\mathbf{x})$ is the translational cell diffusivity tensor, $n(\mathbf{x})$ is the local cell concentration, $p_e(\mathbf{x})$ is the excess pressure, v is the mean volume of a cell, $\Delta\rho$ is the the difference between the cell and fluid density, ρ is the fluid density, $\mathbf{g}$ is the acceleration due to gravity and μ is the fluid viscosity. Both $\langle \mathbf{p} \rangle$ and $\mathbf{D}$ require a knowledge of the probability distribution function of cell swimming directions, $f(\mathbf{p})$, at each point in the fluid as a function of the unit cell swimming direction vector, $\mathbf{p}$. $f(\mathbf{p})$ is modelled using a Fokker-Planck equation of the form (Pedley & Kessler 1990)

$$\frac{\partial f}{\partial t} + \nabla \cdot (\dot{\mathbf{p}} f) = D_r \nabla^2 f, \tag{4}$$

where D_r is the cells' rotational diffusivity. D_r encompasses all the possible sources of rotational diffusivity including both Brownian effects as well as the intrinsically stochastic, locomotory apparatus of the cells themselves. The deterministic torque balance associated with a cell in a flow field can be expressed (from Pedley & Kessler 1990) as

$$\dot{\mathbf{p}} = \frac{1}{2B} \left[\mathbf{k} - (\mathbf{k} \cdot \mathbf{p})\mathbf{p} \right] + \frac{1}{2} \mathbf{\Omega} \wedge \mathbf{p} + \alpha_0 \mathbf{p} \cdot \mathbf{E} \cdot (\mathbf{I} - \mathbf{pp}), \tag{5}$$

where α_0 is the cell eccentricity, $\mathbf{\Omega} = \nabla \wedge \mathbf{u}$ is the fluid vorticity, $\mathbf{E}$ is the rate-of-strain tensor and B is the gyrotactic orientation parameter. B represents a reorientation time scale due to the balance between viscous and gravitational torques, given by

$$B = \frac{\mu\alpha_\perp}{2h\rho g}, \tag{6}$$

where h is the offset of the centre of mass from the geometrical centre and $\alpha_\perp$ is the dimensionless resistance coefficient for rotation about an axis perpendicular to $\mathbf{p}$ (Pedley & Kessler 1990). Following Pedley & Kessler (1990) and Bees *et al.* (1998b), we can calculate

$$\langle \mathbf{p} \rangle = \int_S \mathbf{p} f \, dS, \tag{7}$$

where S is the surface of the unit sphere. If we assume (as in Pedley & Kessler 1990) that there exists a constant cell direction correlation time, τ, in which the cell settles to a new preferred orientation, then the diffusivity can be approximated by

$$\mathbf{D} = V_s^2 \tau \left(\langle \mathbf{pp} \rangle \mathcal{N} - \langle \mathbf{p} \rangle^2 \right) \tag{8}$$

where

$$\mathcal{N} = \frac{\langle V^2 \rangle}{V_s^2}. \tag{9}$$

The distribution of swimming speeds for *C. nivalis* is obtained from the experimental data of Hill & Häder (1997). This is used to calculate the mean swimming speed, $V_s \approx 65$ μm s^{-1}, the mean square of the swimming speed, $\langle V^2 \rangle$, and $\mathcal{N}$, which is found to be approximately 1.3. (Note that $\mathcal{N}$ is bounded below by 1.0.) Non-dimensionalizing time with the cell direction correlation time, τ, velocity with V_s, length with $V_s \tau$, concentration with the average cell concentration, $\bar{n}$, and thus $\mathbf{D}$ with $V_s^2 \tau$ (following Pedley *et al.* 1988), the governing equations become

$$\nabla \cdot \mathbf{u} = 0, \tag{10}$$

$$\partial_t \mathbf{u} + \mathbf{u} \cdot \nabla \mathbf{u} = -\nabla p_e - \mathrm{Ri}\, n \mathbf{k} + \frac{1}{\mathrm{Re}} \nabla^2 \mathbf{u} \tag{11}$$

and

$$\partial_t n = -\nabla \cdot \left[n \left(\mathbf{u} + \langle \mathbf{p} \rangle \right) - \mathbf{D} \cdot \nabla n \right]. \tag{12}$$

The ratio of buoyancy to inertia, often called the Richardson number (Drazin & Reid 1982), is given by

$$\mathrm{Ri} = \frac{\bar{n} v \Delta \rho g \tau}{\rho V_s} \tag{13}$$

and the micro-organism Reynolds number is defined as

$$\mathrm{Re} = \frac{\tau V_s^2 \rho}{\mu}. \tag{14}$$

The non-dimensional gyrotaxis parameter is given by

$$\eta = \frac{B}{\tau} \tag{15}$$

and occurs in the non-dimensionalized Fokker-Planck Equation, as does λ, which is given by

$$\lambda = \frac{1}{2BD_r}. \tag{16}$$

Table 1 summarizes the parameters described in this section and details two realistic sets of values as discussed in Bees (1996) and Bees & Hill (1998). For the subsequent analysis, the problem will be simplified by assuming that the cells are spherical, which means that the cell eccentricity, α_0, is zero. Analytic solutions to the gyrotactic Fokker-Planck equation will be used throughout. They were derived for a two-dimensional flow in a vertical plane by Bees (1996) and Bees *et al.* (1998b) and are valid for all values of η, $\mathcal{N}$ and the non-dimensional vorticity, $\omega(\mathbf{x})$. They are

$$\langle \mathbf{p} \rangle^x(\eta, \omega(\mathbf{x})) = \langle \mathbf{p} \rangle^x(\eta\omega) = \frac{4\pi}{3} A_1^1(\eta\omega), \tag{17}$$

$$\langle \mathbf{p} \rangle^z(\eta, \omega(\mathbf{x})) = \langle \mathbf{p} \rangle^z(\eta\omega) = \frac{4\pi}{3} A_1^0(\eta\omega), \tag{18}$$

$$\mathbf{D}^{xx}(\eta, \omega(\mathbf{x}), \mathcal{N}) = \mathbf{D}^{xx}(\eta\omega) = \frac{1}{3}\mathcal{N} + \pi\left[-\frac{4}{15}A_2^0(\eta\omega)\mathcal{N} + \frac{8}{5}A_2^2(\eta\omega)\mathcal{N} - \frac{16\pi}{9}(A_1^1(\eta\omega))^2\right] \tag{19}$$

and

$$\mathbf{D}^{xz}(\eta, \omega(\mathbf{x}), \mathcal{N}) = \mathbf{D}^{xz}(\eta\omega) = \frac{4\pi}{5}A_2^1(\eta\omega)\mathcal{N} - \frac{16\pi^2}{9}A_1^1(\eta\omega)A_1^0(\eta\omega), \tag{20}$$

where

$$\begin{pmatrix} 0 \\ \omega \\ 0 \end{pmatrix} = \nabla \wedge \mathbf{u}. \tag{21}$$

The functions $A_j^i(\eta\omega)$ are given in the Appendix, the superscripts x and z indicate the x- and z-components and for brevity, the $\mathcal{N}$-dependence is only given explicitly when necessary. In particular, we introduce the shorthand

$$E(\eta\omega) = -\langle \mathbf{p} \rangle^x(\eta\omega) \quad \text{and} \quad A(\eta\omega) = \mathbf{D}^{xx}(\eta\omega). \tag{22}$$

3 Linear analysis

On perturbing the uniform solution in a suspension of infinite depth by making the substitutions $\mathbf{u} = \delta\mathbf{u}^1$ and $n = 1 + \delta n^1$ in Equations (10) to (12), where $\delta \ll 1$, we can establish its linear stability. Eliminating the pressure term, we obtain an equation for the z-component of $\mathbf{u}^1$:

$$\partial_t \left(\nabla^2 u_3^1\right) = \frac{1}{\mathrm{Re}}\nabla^4 u_3^1 - \mathrm{Ri}\,\nabla^2 n^1 + \mathrm{Ri}\,\partial_3\partial_3 n^1. \tag{23}$$

Equation (12) becomes

$$\partial_t n^1 + \langle\mathbf{p}\rangle^z(0)\partial_z n^1 - \mathbf{D}^{xx}(0)\partial_x^2 n^1 - \mathbf{D}^{zz}(0)\partial_z^2 n^1 = \eta\mathcal{D}\langle\mathbf{p}\rangle^x(0)\nabla^2 u_3^1, \tag{24}$$

where $D^{zz}(0)$ and $D^{xx}(0)$ are vertical and horizontal diffusivities for the zero flow solution and

$$\mathcal{D}\langle\mathbf{p}\rangle^x(0) = \left.\frac{d\langle\mathbf{p}\rangle^x(\zeta)}{d\zeta}\right|_{\zeta=0}. \tag{25}$$

Consider normal mode solutions of the form

$$u_3^1 = C_u e^{\sigma t + i(kx+mz)} \quad \text{and} \quad n^1 = C_n e^{\sigma t + i(kx+mz)}, \tag{26}$$

where C_u and C_n are constants. Eliminating C_u and C_n gives

$$\begin{aligned} \sigma^2 + \left(im\langle\mathbf{p}\rangle^z(0) + D^{xx}(0)k^2 + D^{zz}(0)m^2 + \frac{k^2+m^2}{\mathrm{Re}}\right)\sigma \\ + \frac{k^2+m^2}{\mathrm{Re}}\left(im\langle\mathbf{p}\rangle^z(0) + D^{xx}(0)k^2 + D^{zz}(0)m^2\right) - \mathrm{Ri}\eta k^2\mathcal{D}\langle\mathbf{p}\rangle^x(0) &= 0. \end{aligned} \tag{27}$$

This is a rewritten form of the equations found by Pedley *et al.* (1988) and the subsequent analysis in this section can be compared with their results. Writing $\sigma = \sigma_R + i\sigma_I$ and solving for σ_R and σ_I gives

$$\sigma_I = -\left(\frac{\dfrac{k^2+m^2}{\mathrm{Re}}m\langle\mathbf{p}\rangle^z(0) + m\langle\mathbf{p}\rangle^z(0)\sigma_R}{D^{xx}(0)k^2 + D^{zz}(0)m^2 + \dfrac{k^2+m^2}{\mathrm{Re}} + 2\sigma_R}\right) \tag{28}$$

and

$$\sigma_R^2 - F_4^2\frac{(F_2+\sigma_R)^2}{(F_1+F_2+2\sigma_R)^2} + F_4\frac{(F_2+\sigma_R)}{(F_1+F_2+2\sigma_R)} + (F_1+F_2)\sigma_R + F_1F_2 - F_3 = 0 \tag{29}$$

where $F_1 = D^{xx}(0)k^2 + D^{zz}(0)m^2$, $F_2 = (k^2+m^2)/\mathrm{Re}$, $F_3 = \mathrm{Ri}\,\eta k^2\mathcal{D}\langle\mathbf{p}\rangle^x(0)$ and $F_4 = m\langle\mathbf{p}\rangle^z(0)$. The neutral curve for modes with zero linear growth is given by $\sigma_R = 0$. This implies

$$(F_1+F_2)^2(F_1F_2 - F_3) + F_4^2F_1F_2 = 0. \tag{30}$$

For no vertical variation $m = 0$, and then

$$k^2 = \frac{K\mathcal{D}\langle \mathbf{p} \rangle^x(0)}{D^{xx}(0)}, \tag{31}$$

where

$$K = \mathrm{Ri}\,\mathrm{Re}\,\eta \tag{32}$$

(see Figure 1). But if $m \neq 0$ then the neutral curve is given by the relationship

$$K = \frac{(k^2+m^2)(D^{xx}(0)k^2 + D^{zz}(0)m^2)}{k^2\mathcal{D}\langle \mathbf{p} \rangle^x(0)} \left(1 + \frac{m^2\langle \mathbf{p} \rangle^z(0)}{\left(\frac{k^2+m^2}{\mathrm{Re}} + D^{xx}(0)k^2 + D^{zz}(0)m^2\right)^2} \right), \tag{33}$$

and on this curve σ has an imaginary part given by Equation (28) and thus the perturbation is oscillatory. Hence, the curve in Figure (1) represents a Hopf bifurcation and it is apparent that K_c, the critical value of K, decreases with m. The curve with the lowest value of K_c occurs when $m = 0$ and here the neutral curve represents a stationary bifurcation. In this case, the linear growth rate of a slightly supercritical mode may be rewritten, using Equations (17) and (19), as

$$\sigma = -\frac{k^2}{2\mathrm{Re}}\left(A(0)\mathrm{Re} + 1\right) \pm \frac{k}{2\mathrm{Re}}\sqrt{k^2\left(A(0)\mathrm{Re} - 1\right)^2 - 4\mathrm{Re}KE'(0)}, \tag{34}$$

where the prime indicates the first derivative, and is plotted in Figure (2). This expression will be expanded in Section 5 to motivate the scalings for a weakly non-linear analysis.

4 The long vertical wavelength equations

We can exploit the long length scale in the z-direction by scaling z with a small parameter, ϵ. First, consider a two dimensional solution in the xz-plane and put $\mathbf{u} = \mathrm{curl}(-\psi\mathbf{j})$, where ψ is the stream function. Then $u = \partial_z\psi$, $w = -\partial_x\psi$ and $\omega = \nabla^2\psi$. Equations (10) to (12) give

$$\partial_t\nabla^2\psi - \frac{1}{\mathrm{Re}}\nabla^4\psi + J(\nabla^2\psi, \psi) = \mathrm{Ri}\,\partial_x n \tag{35}$$

and

$$\partial_t n + J(n,\psi) + \nabla\cdot\left(n\langle \mathbf{p} \rangle(\eta\nabla^2\psi)\right) - \nabla\cdot\left(\mathbf{D}(\eta\nabla^2\psi)\cdot\nabla n\right) = 0 \tag{36}$$

where J is the Jacobian defined by

$$J(n,\psi) = \partial_x n\ \partial_z\psi - \partial_z n\ \partial_x\psi. \tag{37}$$

Putting $Z = \epsilon z$, we obtain

$$\partial_t(\partial_x^2 + \epsilon^2\partial_Z^2)\psi - \frac{1}{\mathrm{Re}}(\partial_x^2 + \epsilon^2\partial_Z^2)^2\psi + \epsilon\partial_Z\psi(\partial_x^2 + \epsilon^2\partial_Z^2)\partial_x\psi - \epsilon\partial_x\psi(\partial_x^2 + \epsilon^2\partial_Z^2)\partial_Z\psi = \mathrm{Ri}\,\partial_x n \tag{38}$$

and

$$\partial_t n + \epsilon\partial_Z\psi\partial_x n - \epsilon\partial_x\psi\partial_Z n + \begin{pmatrix} \partial_x \\ \epsilon\partial_Z \end{pmatrix} \cdot (n\langle\mathbf{p}\rangle(\eta\omega)) - \begin{pmatrix} \partial_x \\ \epsilon\partial_Z \end{pmatrix} \cdot \left[\mathbf{D}(\eta\omega) \cdot \begin{pmatrix} \partial_x \\ \epsilon\partial_Z \end{pmatrix} n\right] = 0 \tag{39}$$

where $\eta\omega = \eta(\partial_x^2 + \epsilon^2\partial_Z^2)\psi$. We write

$$n(x, Z, t) = n^0(x, Z, t) + \epsilon n^1(x, Z, t) + ... \tag{40}$$

and

$$\psi(x, Z, t) = \psi^0(x, Z, t) + \epsilon\psi^1(x, Z, t) + ... \tag{41}$$

where n^i and ψ^i $(i = 0, 1, ...)$ are in general determined by non-linear partial differential equations in terms of the dependent variables. To zero order in ϵ,

$$\partial_t\partial_x^2\psi^0 - \frac{1}{\mathrm{Re}}\partial_x^4\psi^0 = \mathrm{Ri}\partial_x n^0 \tag{42}$$

and

$$\partial_t n^0 + \partial_x\left(\langle\mathbf{p}\rangle^{0x} n^0\right) - \partial_x\left(\mathbf{D}^{0xx}\partial_x n^0\right) = 0, \tag{43}$$

where we have used

$$\langle\mathbf{p}\rangle^x = \langle\mathbf{p}\rangle^{0x} + \epsilon\langle\mathbf{p}\rangle^{1x} + O(\epsilon^2) \tag{44}$$

and similarly for $\mathbf{D}^{xx}$. Here, the superscript 0 means zeroth order in ϵ and x means the x-component. These equations are the same as if we had just assumed no vertical variation, but all the functions of integration in the solution will depend on Z and can be determined from the solvability conditions at higher orders. Rewriting these equations, with the "effective vorticity"

$$p = \eta\partial_x^2\psi^0 = \eta\omega + O(\epsilon), \tag{45}$$

gives

$$\mathrm{Re}\,\partial_t p = \partial_x\left(\partial_x p + K n^0\right) \tag{46}$$

and

$$\partial_t n^0 = \partial_x \left(A(p) \partial_x n^0 + E(p) n^0 \right). \tag{47}$$

The linear analysis of the previous section could be repeated here by further expanding in the x-direction. Equations (46) and (47) are the governing equations for bioconvection patterns in the form of rolls which are independent of the y-direction and are of large vertical aspect ratio. They are nonlinear partial differential equations and solutions of these equations are studied in the following sections. Equations at the next order of ϵ determine the z dependence of the solutions and are investigated in Section 8.

5 Amplitude equations for long vertical wavelength instabilities

As unstable linear disturbances grow in an exponential fashion, non-linear terms become more and more significant. Translational invariance in space, $x \to x + \hat{x}$, implies that the evolution equation of any instability of the amplitude, A, of a solution must be invariant under the transformation $A \to Ae^{i\hat{k}\hat{x}}$, and hence the first translationally invariant term to appear up to third order is $|A|^2 A$. Eventually, the third order terms are of a comparable order to the first order terms and may affect the growth of the solution. If third order terms counteract the linear growth then the bifurcation to instability is said to be supercritical. If, however, the third order terms aid the growth of the linear disturbance then the bifurcation is said to be subcritical and one must look to higher orders in order to saturate the growth of the leading order terms. Subcritical bifurcations may imply the existence of stable bioconvecting solutions below the critical parameter value and, hence, below the neutral curve. See, for example, Coullet & Fauve (1985) and Fauve (1985) for discussions on amplitude equations, and Buzano & Golubitsky (1983) and Golubitsky *et al.* (1984) for the general form of amplitude equations subject to spatial symmetrical constraints. It is possible, in most systems, to generate a long wavelength theory of the evolution of initial disturbances close to the critical point (see Childress & Spiegel 1978 , Chapman & Proctor 1980 and Knobloch 1990). However, due to the fact that the critical values of K and k are zero, we are unable to find such an amplitude equation and, at best, the linear theory is recovered at each attempt. We choose instead to derive a Landau equation (Schlüter *et al.* 1965) which describes the weakly non-linear behaviour of the system at a point (k, K) close to a general point on the neutral curve (k_c, K_c), for

which $k_c \neq 0$, and to investigate the nature of the bifurcation to instability close to the critical point at $k_c = K_c = 0$.

First we will motivate our scaling by expanding the growth rate of Equation (34) in terms of $(K - K_c)$ and $(k - k_c)$,

$$\sigma = \left(\frac{\partial \sigma}{\partial K}\right)_c (K - K_c) + \left(\frac{\partial \sigma}{\partial k}\right)_c (k - k_c) + h.o.t. \tag{48}$$

where the subscript c implies that the function is evaluated at a point on the neutral curve. We find that

$$\sigma = \left(-\frac{E'(0)}{A(0)\mathrm{Re} + 1}\right)(K - K_c) + \left(-\frac{2A(0)k_c}{A(0)\mathrm{Re} + 1}\right)(k - k_c) + h.o.t. \tag{49}$$

where k_c is found from the linear analysis to be $k_c = \sqrt{\frac{-K_c E'(0)}{A(0)}}$. Suppose that the amplitude of a solution on the neutral curve is given by $f(x,t)$, then multiplying Equation (49) by the Fourier-Laplace transform of $f(x,t)$, $\hat{f}(k,\sigma)$, and taking the inverse Fourier-Laplace transform gives the leading order form of the amplitude equation for small but finite amplitude disturbances (see Fauve 1985):

$$\frac{\partial f}{\partial t} = \left(-\frac{E'(0)}{A(0)\mathrm{Re} + 1}\right)(K - K_c) f + \left(\frac{2A(0)k_c}{A(0)\mathrm{Re} + 1}\right) i \frac{\partial f}{\partial x} + h.o.t. \tag{50}$$

This indicates that we should scale time, $1/(K - K_c)$ and x by the same small scale. We also need to scale p such that the higher order terms appear in the equations at the same order as the terms in Equation (50) above. Defining our small parameter δ (where $1 \gg \delta \gg \epsilon$) by

$$\delta^2 K_2 = (K - K_c) + O(\delta^3) \tag{51}$$

where K_2 measures the distance from criticality, then this leads us to the scalings and expansions

$$\begin{aligned} T &= \delta^2 t \\ X &= \delta^2 x \\ \partial_x &\longmapsto \partial_x + \delta^2 \partial_X \\ n^0(x,X,T) &= 1 + \delta n_1(x,X,T) + \delta^2 n_2(x,X,T) + ... \\ p(x,X,T) &= \delta p_1(x,X,T) + \delta^2 p_2(x,X,T) + ... \end{aligned} \tag{52}$$

and, for now, consider

$$K = K_c + \delta K_1 + \delta^2 K_2 + \delta^3 K_3 + ... \tag{53}$$

where we shall show that $K_1 = 0$. As E is odd and A is even, we can write

$$E(p) = \left(\delta p_1 + \delta^2 p_2 + ...\right) E'(0) + \frac{1}{3!}\left(\delta^3 p_1^3 + ...\right) E'''(0) + ... \tag{54}$$

and

$$A(p) = A(0) + \frac{1}{2}\left(\delta^2 p_1^2 + 2\delta^3 p_1 p_2 + \delta^4 p_2^2 + ...\right) A''(0) + ... \tag{55}$$

Hence, substituting these expansions and scalings into Equations (46) and (47) gives

$$\begin{aligned}\mathrm{Re}\,\delta^3 \partial_T \left(p_1 + \delta p_2 + ...\right) &= \delta\left(\partial_x^2 + 2\delta^2 \partial_x \partial_X + \delta^4 \partial_X^2\right)\left(p_1 + \delta p_2 + ...\right) \\ &+\delta\left(K_c + \delta K_1 + \delta^2 K_2 + ...\right)\left(\partial_x + \delta^2 \partial_X\right)\left(n_1 + \delta n_2 + \delta^2 n_3\right)\end{aligned} \tag{56}$$

and

$$\begin{aligned}&\delta^3 \partial_T \left(n_1 + \delta n_2 + ...\right) = \\ &\delta\left(\partial_x + \delta^2 \partial_X\right)\left[\left(\left(p_1 + \delta p_2 + ...\right) E'(0) + \frac{1}{3!}\left(\delta^2 p_1^3 + ...\right) E'''(0) + ...\right)\left(1 + \delta n_1 + \delta^2 n_2 + ...\right)\right. \\ &\left. + \left(A(0) + \frac{1}{2} A''(0)\left(\delta^2 p_1^2 + ...\right)\right)\left(\partial_x + \delta^2 \partial_X\right)\left(n_1 + \delta n_2 + \delta^2 n_3 + ...\right)\right].\end{aligned} \tag{57}$$

The lowest orders of Equations (56) and (57) are

$$\partial_x^2 p_1 + K_c \partial_x n_1 = 0 \tag{58}$$

and

$$E'(0)\partial_x p_1 + A(0)\partial_x^2 n_1 = 0 \tag{59}$$

which imply that

$$\begin{pmatrix} p_1 \\ n_1 \end{pmatrix} = f(X,T) \begin{pmatrix} -\frac{A(0)ki}{E'(0)} \\ 1 \end{pmatrix} e^{ikx} + c.c. \tag{60}$$

where $k = 0$ or $\sqrt{\frac{-K_c E'(0)}{A(0)}}$. This defines the piecewise continuous neutral curve seen in Figure (1). We choose to take the non-trivial root and, hence, consider a solution near that part of the neutral curve that gives spatial pattern. If K_c is small then this solution is close to the trivial critical solution at $k = 0$. The next order gives the two equations

$$\partial_x^2 p_2 + K_c \partial_x n_2 = -K_1 \partial_x n_1 \tag{61}$$

and

$$E'(0)\partial_x p_2 + A(0)\partial_x^2 n_2 = -E'(0)\partial_x \left(p_1 n_1\right). \tag{62}$$

Clearly $\partial_x n_1$ is a secular term and $\partial_x \left(p_1 n_1\right)$ is not. Solvability implies that the secular term is orthogonal to the solution of the homogeneous equation and so, in this case, the secular term should vanish and, hence, $K_1 = 0$. This is consistent with our predicted scalings (Equation (51)). The general solution for these equations is

$$\begin{pmatrix} p_2 \\ n_2 \end{pmatrix} = f_2(X,T) \begin{pmatrix} a \\ b \end{pmatrix} e^{ikx} + g(X,T) \begin{pmatrix} d \\ e \end{pmatrix} e^{2ikx} + c.c. \tag{63}$$

We choose $a = b = 0$ as this part of the solution can be combined with the leading order solution. Substituting Equation (63) back in to Equations (61) and (62), we get that

$$g(X,T) = f^2(X,T), \tag{64}$$

$$d = \frac{ikA(0)}{6E'(0)} \qquad \text{and} \qquad e = \frac{1}{3}. \tag{65}$$

The next order gives

$$\partial_x^2 p_3 + K_c \partial_x n_3 = Re\partial_T p_1 - K_2 \partial_x n_1 - K_c \partial_X n_1 - 2\partial_x \partial_X p_1 \tag{66}$$

and

$$\begin{aligned} &E'(0)\partial_x p_3 + A(0)\partial_x^2 n_3 = \partial_T n_1 - E'(0)\partial_x \left(p_2 n_1\right) - E'(0)\partial_x \left(p_1 n_2\right) \\ &-E'(0)\partial_X p_1 - 2A(0)\partial_x \partial_X n_1 - \frac{1}{2}A''(0)\partial_x \left[p_1^2 \partial_x n_1\right]. \end{aligned} \tag{67}$$

The solvability condition (see Ince 1956, §9.34) requires that

$$\int_0^{\frac{2\pi}{k}} \mathbf{u}^H \mathbf{N} dx = 0 \tag{68}$$

where H means the Hermitian, $\mathbf{u}$ is the solution to the adjoint problem and $\mathbf{N}$ indicates the secular terms in the inhomogeneous problem. Hence,

$$f_T = \left(\frac{-K_2 E'(0)}{A(0)\mathrm{Re}+1}\right) f - \left(\frac{-K_c E'(0) + 9K_c^2 A''(0)}{6(A(0)\mathrm{Re}+1)}\right) |f|^2 f + \left(\frac{2\sqrt{-K_c E'(0) A(0)}}{A(0)\mathrm{Re}+1}\right) i f_X \tag{69}$$

(and a conjugate equation for the complex conjugate of f) which represents the non-linear saturation of linear modes.

The if_X term is invariant to all of the relevant symmetries and is a consequence of prescribing a periodic domain of size $L = 2\pi/k_c$. The term represents corrections to the amplitude equation for small variations of the wavenumber from k_c and can be removed by the transformation

$$\begin{pmatrix} X' \\ T' \end{pmatrix} = \begin{pmatrix} X + i\kappa T \\ T \end{pmatrix}, \tag{70}$$

where

$$\kappa = \left(\frac{2\sqrt{-K_c E'(0) A(0)}}{A(0)\mathrm{Re} + 1} \right), \tag{71}$$

so that

$$f_T \longrightarrow f_{T'} + i\kappa f_{X'}. \tag{72}$$

For the special case at the critical point, where $k = 0$, the if_X term vanishes. As K_c decreases to zero, the third order term tends to zero but, crucially, does so from below. The multiplier of the $|f|^2 f$ term is negative provided $K_c > 0$ and

$$E'(0) < 9K_c A''(0). \tag{73}$$

$E'(0)$ is always negative and $A''(0)$ is positive, provided $A(p)$ has a minimum at $p = 0$. This occurs if and only if $\mathcal{N} > 1.0206$ (see Equations 9 and 19). Hence, if either $\mathcal{N} > 1.0206$ (very likely) or K_c is small but positive, then the multiplier of the $|f|^2 f$ term is negative. We conclude that the bifurcation to instability is supercritical and this is our main result in this section. It implies that the linear analysis is useful for predicting the wavenumber of the initial disturbance from equilibrium.

6 Steady non-linear solutions

We look for steady periodic solutions to the long vertical wavelength Equations (46) and (47). The time-independent equations can be integrated directly to obtain

$$p_x + K\left(n^0 - \Lambda\right) = 0 \tag{74}$$

and

$$A(p) n^0_x + E(p) n^0 = C_2 \tag{75}$$

where C_2 and Λ are in general unknown functions of Z. Applying the symmetry condition $p = 0$ when $n^0_x = 0$ (i.e. that vorticity is zero in the centre of the plume) gives $C_2 \equiv 0$. In general n^0 and p are functions of Z. To prepare the ground for later sections, we renormalise n^0 as follows. Integrating the first equation over x and assuming periodic solutions, we find that

$$\left\{n^0\right\}^x = \Lambda(Z) \tag{76}$$

where $\{\cdot\}^x$ is a space average over x (i.e. $\left\{n^0\right\}^x \equiv l^{-1}\int_0^l n^0 dx$, where l is the wavelength of the periodic solution, n^0). As n^0 is the normalized cell concentration, so

$$\left\{\left\{n^0\right\}^x\right\}^Z = \left\{\Lambda(Z)\right\}^Z = 1. \tag{77}$$

We introduce the change of variables

$$N = \frac{n^0}{\Lambda(Z)} \tag{78}$$

and

$$K^*(Z) = \Lambda(Z)K \tag{79}$$

such that

$$\{N\}^x = 1. \tag{80}$$

This implies that the long vertical wavelength equations, (46) and (47), become

$$\mathrm{Re}\, p_t = \left(p_x + K^*\left(N - 1\right)\right)_x \tag{81}$$

and

$$N_t = \left(A(p)N_x + E(p)N\right)_x, \tag{82}$$

where there is now only one parameter, $K^*(Z)$. By changing variables, such that $q = \ln(N)$, we see that the time-independent equations are Hamiltonian and can be written as $\partial_x p_= - \partial_q \mathcal{H}$ and $\partial_x q = \partial_p \mathcal{H}$, where

$$\mathcal{H} = K^*\left(e^q - q\right) - \int_0^p \frac{E(p')}{A(p')}dp', \tag{83}$$

and therefore the trajectories are closed, indicating many periodic orbits as expected.

The steady versions of Equations (81) and (82) can be written in the form

$$p_x = K^*(1 - N) \tag{84}$$

and

$$N_x = -\frac{E(p)}{A(p)}N, \tag{85}$$

and are integrated numerically using a fourth order Runge-Kutta scheme. Examples of the closed orbits of this system are shown in Figure (3) and clearly there are an infinity of possible solutions but their wavenumbers are restricted to a small range from zero to some maximum value obtained by observation from the numerical solutions. Thus, in a periodic domain of a specified size, there are finitely many steady state solutions. Figure (4) displays examples of the periodic curves of $q(x)$ for $K^* = 0.1$, and shows how they increase their wavelength with increasing amplitude. For all values of K^* the pattern wavelength increases with its amplitude. Therefore, small amplitude solutions give the maximum wavenumber. The small amplitude solutions are precisely those given by the linear analysis of Section 3. Hence, the maximum wavenumber is given by

$$k_c = \sqrt{\frac{-K_c E'(0)}{A(0)}}, \tag{86}$$

from Equation (31). This is consistent with the form of the amplitude equation given in Section 5. However, the system is structurally unstable in that if a small perturbation displaces a solution from one trajectory to another then it will stay on the new trajectory. For bioconvection in an infinite domain we do not know the final pattern unless we know every perturbation from the homogeneous state. It is thus necessary to consider higher orders in order to establish the stability of the greater system. However, for bioconvection with finite horizontal extent, the above analysis provides us with a finite number of steady solutions dictated by the maximum wavenumber, k_c. Furthermore, we see in Figure (4) that the maximum amplitudes of the concentration profiles become larger as the wavelength increases. Clearly there is a physical maximum concentration due to the non-zero volume of the individual cells, approximately $5 \times 10^{-10}\, cm^3$. This is, in general, further reduced due to geometrical constraints on the packing arrangement. Hence, there is an upper bound on the concentration of 2×10^9 cells per cm^3 and this will provide an upper bound on the pattern wavelength. However, this wavelength is unlikely to be realized as cell-to-cell interactions become more important as the concentration increases. Such interactions are beyond the scope of this paper (but see Bees *et al.* 1998a).

Here we have shown, that it is possible to construct steady state solutions from the first order equations

that are non-linear in x and describe a horizontal balance between diffusion and gyrotaxis. These solutions are only dependent on Z through the functions of integration, and they will be used in later sections when investigating the system at higher orders.

7 Horizontally drifting plumes

In certain special situations it is possible to obtain time-dependent solutions. In this section we present an illustrative example of a solution that may help to explain why some plume structures drift in a regular fashion. In particular, we investigate a travelling wave solution that leaves in its path a regular array of drifting plumes. It is first necessary to break the symmetry of the system and impose a "background vorticity", by requiring that the effective vorticity, p, equals p_0 at $x = \infty$ where p_0 is a positive constant. For example, a constant shear flow in the horizontal direction would be sufficient.

Consider $\Xi = x - ct$, where without loss of generality $c \geq 0$, then the long vertical wavelength equations (81) and (82) become

$$-c\,\mathrm{Re}\,p' = (p' + K^* N)' \tag{87}$$

and

$$-cN' = (A(p)N' + E(p)N)' \tag{88}$$

where the prime indicates differentiation with respect to Ξ. This implies that

$$p' = K^*(1 - N) - c\,\mathrm{Re}\,p + C_1 \tag{89}$$

and

$$N' = -\frac{E(p)N + cN + C_2}{A(p)}. \tag{90}$$

For a rightward travelling wave, we look for solutions that are homogeneous far enough to the right such that $N = 1$, $p = p_0$ and $N' = p' = 0$ at $\Xi = \infty$. As N represents the concentration of cells, so $N \geq 0 \ \ \forall\, \Xi \in \mathbb{R}$, which means that no trajectory that asymptotes to $(p, N) = (p_0, 1)$ should cross the line in phase space given by $N = 0$. Applying the boundary conditions at $\Xi = \infty$ to Equation (89) implies that $C_1 = c\,\mathrm{Re}\,p_0$. Applying boundary conditions to Equation (90) gives

$$c + C_2 = -E(p_0). \tag{91}$$

This enables us to rewrite the equations as

$$p' = cRe(p_0 - p) + K^*(1 - N) \tag{92}$$

and

$$N' = \frac{[c\,(1-N) + (E(p_0) - E(p)N)]}{A(p)}. \tag{93}$$

Hence, there is an equilibrium point at $(p_0, 1)$. Linearizing about this point and calculating the eigenvalues, λ, corresponding to the principal linear growth rates, we find that

$$\lambda = -\frac{1}{2}\left(c\mathrm{Re} + \frac{c + E(p_0)}{A(p_0)}\right) \pm \frac{1}{2}\sqrt{\left(c\mathrm{Re} - \frac{c + E(p_0)}{A(p_0)}\right)^2 + 4K^*\frac{E'(p_0)}{A(p_0)}}, \tag{94}$$

which implies that there is a stable (with respect to Ξ) focus or node, or a saddle point depending on $E(p_0)$ etc. The stable focus represents growing oscillations travelling to the right but the other two cases lead to unbounded cell concentrations and will not be considered further. For the stable focus to exist we require $\Re(\lambda) < 0$, which implies that

$$0 \leq \frac{-E(p_0)}{A(p_0)\mathrm{Re} + 1} < c, \tag{95}$$

and $\Im(\lambda) \neq 0$, which implies that

$$c_- < c < c_+ \tag{96}$$

where

$$c_\pm = \frac{E(p_0)}{A(p_0)\mathrm{Re} - 1} \mp \frac{2A(p_0)}{A(p_0)\mathrm{Re} - 1}\sqrt{\frac{-K^*E'(p_0)}{A(p_0)}}. \tag{97}$$

Hence, we require

$$E'(p_0) < 0 \tag{98}$$

for real, non-zero values of $c_\pm$. The nullclines for this system are given by

$$N = \frac{c\mathrm{Re}}{K^*}(p_0 - p) + 1 \tag{99}$$

and

$$N = \frac{c + E(p_0)}{c + E(p)} \tag{100}$$

and are plotted in Figure (5). This figure enables us to see the location of two other equilibrium points and to establish their stability from geometrical considerations. The saddle point is the second most

important feature and it clearly allows the possibility for a homoclinic orbit bifurcation to a limit cycle around the focus (e.g. Balmforth 1995). A Hopf bifurcation may occur and it is the objective of the subsequent analysis to establish necessary and realistic conditions for its existence. If a trajectory starts in the neighbourhood of $(p, N) = (p_0, 1)$, then we also require that $N' \leq 0$ (i.e. $\partial_t N \geq 0$) on $N = 0$ for N to be bounded below by at least $N = 0$. If $N = 0$ then

$$N' = -\frac{C_2}{A(p)} \tag{101}$$

and hence we require that C_2 be positive. This in turn implies that

$$0 \leq c \leq -E(p_0). \tag{102}$$

The maximum wavespeed is given by $c = -E(p_0)$ and occurs when $C_2 = 0$. Clearly no travelling wave solutions exist if there is no background vorticity as $c = 0$ if $p_0 = 0$. Collecting all of these necessary conditions together for a limit cycle to exist gives

$$0 \leq \frac{-E(p_0)}{A(p_0)\mathrm{Re} + 1} < c \leq -E(p_0) \tag{103}$$

and

$$c_- < c < c_+, \tag{104}$$

where

$$c_\pm = \frac{E(p_0)}{A(p_0)\mathrm{Re} - 1} \mp \frac{2A(p_0)}{A(p_0)\mathrm{Re} - 1}\sqrt{\frac{-K^* E'(p_0)}{A(p_0)}} \tag{105}$$

and

$$E'(p_0) < 0 \tag{106}$$

(see Figure 6). As K^* decreases then the region described by Equation (104) shrinks but the region only vanishes if $K^* \leq 0$. Similarly, the region described by Equation (103) decreases as Re decreases but only vanishes if $\mathrm{Re} \leq 0$. The two regions always coincide near to $p^0 = 0$ and $c = 0$. Numerical integration of the governing equations (89) and (90) shows that a limit cycle does exist for certain limited choices of c (see Figures 7 and 8) which corresponds exactly with the region given in Figure 6. This suggests that if the pattern nucleates at a point then plumes will spread out and increase in amplitude until a regular pattern is reached, where the wave speed is confined to a small range. This in turn suggests that

laminar fluid motions can control the transport and production of plume structures and that there is a limited range of possible transport speeds determined by the physical attributes of the swimming cells. However, the presence of horizontal boundaries will influence both the above solutions and the potential for constructing feasible experiments to compare with the above results.

In order to illustrate the results of this section, we provide an example computation for a suspension of *C. nivalis* in a deep channel bounded by vertical walls 3 cm apart. A shear flow is imposed by moving one of the boundaries. Travelling waves, if they exist, will consist of plumes travelling to the right or left with a speed that is confined to a small range of values. Condition (106) implies that we must look for a value of p_0 that satisfies $E'(p_0) < 0$. Equations (17), (22) and (137) give the necessary constraint on p_0^2 in the form of a cubic equation, which can be solved to give $|p_0| < 1.3$. We choose $p_0 = 1.0$ and, since $p_0 = \eta\omega = \eta\tau\Omega$, and given $\tau = 1.3$ and $\eta = 2.6$ from Table 1, we find that the magnitude of the dimensional vorticity, Ω, is 0.3 s^{-1}. Taking into account that $\Omega = \nabla \wedge \mathbf{u} \approx w_x$ and that the distance between the boundaries equals 3 cm, one of the boundaries must move at a speed of 0.9 cm s^{-1}. From Table 1, $\mathrm{Re} = 5.2 \times 10^{-5}$, $\mathrm{Ri} = 5.2 \times 10^{-6} n_0$ and $\mathcal{N} = 1.3$. Taking $\bar{n} = 10^6$ cells cm^{-3} and assuming zero vertical variation in the plume profile, Equations (103) and (104) give (to 6 s.f. to illustrate the small range of possible values)

$$0.300550 < c < 0.300556 \tag{107}$$

and

$$0.290827 < c < 0.310295, \tag{108}$$

respectively. In dimensional terms, the speed of the travelling plume is approximately 0.0019 cm s^{-1}. Clearly, in the suggested experimental arrangement, it is possible that the close proximity of boundaries may affect the structure of the travelling array of plumes. Increasing the distance between the boundaries may solve this problem but would make such an experiment more difficult to perform, as it implies an associated increase in the speed of the boundaries in order to maintain a particular value of the forcing vorticity. It would also be possible to measure the upper value of vorticity for which travelling plumes still exist. The theoretical critical value is given approximately by $p_0 = 1.3$. Increasing p_0 beyond this value will destroy the travelling plume structure entirely as, on average, the cells start to tumble and

$E'(p_0) > 0$.

8 Vertical variation of the steady state solutions

In this section we develop a theory to help explain the nature of the pulses that travel down the long plume structures (c.f. Kessler 1985a, 1985b). We consider the steady state solutions of Section 6 and allow these solutions to vary slowly with time and in the vertical direction. If we rescale time with the small parameter ϵ, such that $T = \epsilon t$, then we can use the equations of Section 4 to obtain the leading order equations for a small variation in the z direction. The first order equations are (see Section 4 and Equations (42) and (43))

$$\partial_x(\eta\partial_x^2\psi^0) + K\left(n^0 - \Lambda(Z,T)\right) = 0 \tag{109}$$

and

$$A(\eta\partial_x^2\psi^0)n_x^0 + E(\eta\partial_x^2\psi^0)n^0 = C_2(Z,T), \tag{110}$$

where Λ is defined in Section 6 and C_2 is at present an unknown function of Z and T. Applying the symmetry condition, that vorticity be zero ($\partial_x^2\psi^0 = 0$) in the centre of a plume ($n_x = 0$) in which $E(0) = 0$, gives $C_2 = 0$. At second order, we get

$$\frac{1}{\mathrm{Re}}(\partial_x^4\psi^1) + \mathrm{Ri}\,\partial_x n^1 = \partial_T(\partial_x^2\psi^0) + \partial_Z\psi^0\partial_x^3\psi^0 - \partial_x\psi^0\partial_x^2\partial_Z\psi^0 \tag{111}$$

and

$$\begin{aligned}
&\partial_x\left(n^1\langle\mathbf{p}\rangle^{0x}(\eta\partial_x^2\psi^0) + n^0\langle\mathbf{p}\rangle^{1x} - \mathbf{D}^{0xx}(\eta\partial_x^2\psi^0)\partial_x n^1 - \partial_x n^0\mathbf{D}^{1xx}\right)\\
= \;& -\partial_T n^0 + \partial_x\left(\mathbf{D}^{xz}(\eta\partial_x^2\psi^0)\partial_Z n^0\right) + \partial_Z\left(\mathbf{D}^{xz}(\eta\partial_x^2\psi^0)\partial_x n^0 - \langle\mathbf{p}\rangle^z(\eta\partial_x^2\psi^0)n^0\right)\\
&+\partial_x\psi^0\partial_Z n^0 - \partial_Z\psi^0\partial_x n^0,
\end{aligned} \tag{112}$$

where

$$\langle\mathbf{p}\rangle^{1x} = \eta\partial_x^2\psi^1\frac{d}{d\xi}\langle\mathbf{p}\rangle^x(\xi)\Big|_{\xi=\eta\partial_x^2\psi^0} \tag{113}$$

and a similar expression for the linearization, $\mathbf{D}^{1xx}$, of $\mathbf{D}^{xx}$ with respect to the steady state solution. The solvability condition can be found by integrating Equation (112) over a horizontal wavelength. If

$\{\cdot\}^x$ represents a periodic space average in the x-direction as before, then

$$\partial_T \left\{n^0\right\}^x = \partial_Z \left\{\mathbf{D}^{xz}(p)\partial_x n^0 - \langle \mathbf{p}\rangle^z(p) n^0\right\}^x + \left\{\partial_x \psi^0 \partial_Z n^0 - \partial_Z \psi^0 \partial_x n^0\right\}^x, \tag{114}$$

where $p = \eta \partial_x^2 \psi^0$. The last two terms in (114) can be rearranged to give $\partial_Z \left\{n^0 \partial_x \psi^0\right\}^x$, and substituting from (109) gives $-\partial_Z \left\{\partial_x \psi^0 (\eta \partial_x^3 \psi^0 / K - \Lambda(Z,T))\right\}^x \equiv \partial_Z \left\{p^2/K\eta\right\}^x$. Simplifying the other terms in Equation (114) so that they are also written in terms of p and Λ, using the first order equations ((109) and (110)), gives

$$\partial_T \Lambda(Z,T) = \partial_Z \left\{G(p)\Lambda(Z,T) + \frac{p^2}{K\eta}\right\}^x, \tag{115}$$

where

$$G(p) = -\langle \mathbf{p}\rangle^z(p) - \mathbf{D}^{xz}(p)\frac{E(p)}{A(p)}. \tag{116}$$

This equation may possess travelling wave solutions and, in some respects, is similar to the equations discussed by Whitehead (1988) in which soliton-like pulses travel up magma ducts in a viscous matrix. It is the purpose of the following analysis to investigate small amplitude solutions for which the wave speed is derived but not the waveform.

The cell normalization condition implies that $\{\Lambda(Z,T)\}^Z = 1$ and so we write

$$\Lambda(Z,T) = 1 + M(Z,T), \tag{117}$$

where $|M(Z,T)| \ll 1$ and $\{M(Z,T)\}^Z = 0$, and expand p and n^0 in terms of $M(Z,T)$ in Equations (109) and (110) as

$$p(x,Z,T) = p_0(x) + M(Z,T)p_1(x) + O(M^2) \tag{118}$$

and

$$n^0(x,Z,T) = n_0(x) + M(Z,T)n_1(x) + O(M^2). \tag{119}$$

At first order we regain the non-linear equations (84) and (85) for solutions in the horizontal direction with zero vertical variation, i.e.

$$p_{0x} + K\,(n_0 - 1) = 0 \tag{120}$$

and

$$n_{0x} + \frac{E(p_0)}{A(p_0)} n_0 = 0. \tag{121}$$

The next order in $M(Z,T)$ provides a set of linear equations for the perturbations to the steady state solutions which are independent of $M(Z,T)$, Z and T:

$$p_{1x} + K\,(n_1 - 1) = 0 \tag{122}$$

and

$$n_{1x} + \frac{E(p_0)}{A(p_0)} n_1 + \frac{d}{dp_0}\left(\frac{E(p_0)}{A(p_0)}\right) n_0 p_1 = 0. \tag{123}$$

This last system describes a forced oscillator and potentially has solutions with wavelengths that are quotient multiples of the unperturbed system. We can find explicit solutions with a multiple of the wavenumber of the unperturbed system satisfying the same boundary conditions, and so more than one closed orbit is possible for $(p_1,\ n_1)$, for any given solution $(p_0,\ n_0)$.

Using Equations (117) and (118) in Equation (115) gives

$$\partial_T M(Z,T) = \left\{ G'(p_0) p_1 + \frac{2 p_0 p_1}{K\eta} \right\}^x \partial_Z M(Z,T) + O(M^2). \tag{124}$$

For a travelling wave solution, put $\Xi \equiv Z - ct$ in Equation (124) so that

$$\partial_\Xi M(\Xi)\,(\mathcal{B} + c) = 0, \tag{125}$$

where

$$\mathcal{B} = \left\{ G'(p_0) p_1 + \frac{2 p_0 p_1}{K\eta} \right\}^x. \tag{126}$$

Clearly, a non-trivial solution exists when the wave speed is given by $c = -\mathcal{B}$. In principle, the full problem in Equation (115) is sufficient to calculate the waveform but it is not amenable to simple analysis. As an example, we show a numerical example for n_1 and p_1 given that $K = 0.01$ and $n_0 = 5$ when $p_0 = 0$, which is just one of an infinite number of possible orbits. We find a closed orbit with the initial conditions $p_1 = 0$ and $n_1 = 13.8$, as illustrated in Figures (9) and (10), which has the same wavelength as the unperturbed solution. In this example we can use the functions p_0 and p_1 to calculate c.

A possible experimental test of the theory would be to measure the concentration profiles and speeds of small amplitude ($|M| \ll 1$) travelling pulses on otherwise stationary plumes and compare the results with the theory. Experimental observations of pulses indicate that they travel at a speed in the range 0.1–1 mm s^{-1}. Averaging the concentration profiles in the Z direction would give the n_0 profile. From

Section 6 we see that the first order equations, (120) and (121) are Hamiltonian and thus we can use Equation (83) to calculate p_0. Equations (122) and (123) can then be used to solve for (p_1, n_1) and the wavespeed, c, can then be calculated from Equation (125). Alternatively, n_1 can be extracted directly from the cell concentration profile data (i.e. from the profile of the travelling pulse). The wavespeed should be compared with the experimentally determined value. Notice that it is independent of $|M(Z,T)|$ as long as $|M(Z,T)|$ is small. Clearly, the computation of p_0 and p_1 can be avoided if one can measure them directly, instead of n_0 and n_1. As an example, we could calculate the pulse speed from the profiles in Figure 9 as if we had obtained them from experiments (or via calculation from the concentration data). As $c = -\mathcal{B}(p_0, p_1)$, we must first calculate $\mathcal{B}$ from Equation (126) which consists of an integral with respect to x over one wavelength divided by the wavelength. The integrand consists of functions of p_0 and p_1 given by Equations (17) to (20) and (116). The integration can be efficiently performed numerically using commercially available tools such as Maple or Mathematica. Finally, the speed should be expressed in dimensional form by multiplying by $V_s \approx 65 \times 10^{-4}$ cm s^{-1}. For the solutions portrayed in Figure 9, and assuming that $\eta = 2.6$ (Case I of Table 1), $K = 0.01$ and $\mathcal{N} = 1.0$, we find that $c = -1.95$, which corresponds to a speed of 0.13 mm s^{-1} downwards. Using $\eta = 1.3$ (Case II of Table 1) gives $c = -3.89$ and thus the speed is 0.25 mm s^{-1}. Both of these results are for very small amplitude pulses and larger amplitude solutions may travel faster, as observed in the experiments. Even though we have only considered small amplitude pulses, the calculated speeds are certainly realistic.

9 Extension to a three-dimensional flow field

A goal of future work is to investigate the three-dimensional structure of deep bioconvection. Some progress towards this can be made if we assume, as may be suggested by observations, that the vertical component of the vorticity is zero, so that we can use the spherical harmonic approximations developed in Bees *et al.* (1998b) for a three-dimensional flow field with purely horizontal vorticity. Suppose that there is a poloidal velocity field, F, such that

$$\mathbf{u} = \nabla \wedge \nabla \wedge (F\mathbf{k}) \tag{127}$$

which gives

$$\nabla \wedge (F\mathbf{k}) = \begin{pmatrix} \partial_y F \\ -\partial_x F \\ 0 \end{pmatrix}, \tag{128}$$

$$\mathbf{u} = \begin{pmatrix} \partial_x \partial_z F \\ \partial_y \partial_z F \\ \nabla_H^2 F \end{pmatrix} \tag{129}$$

and

$$\omega = \nabla \wedge \mathbf{u} = \begin{pmatrix} -\partial_y \nabla^2 F \\ \partial_x \nabla^2 F \\ 0 \end{pmatrix}, \tag{130}$$

where ∇_H^2 is the horizontal Laplacian. Eliminating the pressure term and applying Equations (128)–(130) to (10)–(12) gives

$$-\partial_t \nabla^2 \nabla_H^2 F = -\mathcal{A}_1(F) - \mathcal{A}_2(F) + \mathrm{Ri}\nabla_H^2 n + \frac{1}{\mathrm{Re}}\nabla^4 \nabla_H^2 F \tag{131}$$

and

$$\partial_t = -\partial_x n \partial_x \partial_z F - \partial_y n \partial_y \partial_z F + \partial_z n \nabla_H^2 F - \nabla \cdot (n\langle \mathbf{p} \rangle - \mathbf{D} \cdot \nabla n), \tag{132}$$

where the non-linear operators, $\mathcal{A}_1(F)$ and $\mathcal{A}_2(F)$, are given in the Appendix. We can now proceed as in Section 4 by introducing a long vertical wavelength, $Z = \epsilon z$ where $\epsilon \ll 1$, to obtain

$$\partial_t \nabla_H^4 F^0 = \mathrm{Ri}\nabla_H^2 n^0 + \frac{1}{\mathrm{Re}}\nabla_H^6 F^0 \tag{133}$$

and

$$\partial_t n^0 = -\nabla_H \cdot \left(n^0 \langle \mathbf{p} \rangle (\nabla_H^2 F^0) - \mathbf{D}(\nabla_H^2 F^0) \cdot \nabla_H n^0 \right), \tag{134}$$

where

$$n(x, Z, t) = n^0(x, Z, t) + \epsilon n^1(x, Z, t) + ... \tag{135}$$

and

$$F(x, Z, t) = F^0(x, Z, t) + \epsilon F^1(x, Z, t) + ... \tag{136}$$

As before, these equations are not explicitly dependent on Z but the functions of integration will be.

The expressions given in Bees *et al.* (1998b) can be used for the terms $\langle \mathbf{p} \rangle$ and $\mathbf{D}$. To proceed further we should have to consider particular forms for n^0 and $\nabla_H^2 F^0$; for example, we may introduce hexagonal or square planforms (see Buzano & Golubitsky 1983 and Golubitsky *et al.* 1984). These equations may be used in future analysis to predict the three-dimensional patterns in gyrotactic bioconvection and to analyse their stability.

10 Discussion

Guided by observations of long plume structures in deep suspensions we have expanded the full equations, describing gyrotactic bioconvection, in the vertical direction. In doing so, we assume that any vertical variation of the horizontal cell concentration and fluid flow fields occurs on long length and time scales. We divide this discussion into two parts that are relevant to the mathematical theory and a biological viewpoint, respectively.

Initially, we analyse the first order set of non-linear partial differential equations by constructing a weakly non-linear theory to show that the bifurcation to instability is supercritical and thus the linear theory can be used to predict the first unstable wavelengths to occur in a well-mixed suspension. In particular, at first order (i.e. with no vertical variation) we obtain a set of partial differential equations in x and t, for which we derive a Landau equation for the non-linear saturation of linear modes close to the curve of neutral stability and show that the bifurcation to instability is supercritical. Further analysis could be carried out on the full non-linear equations, allowing for the Hopf bifurcation resulting from non-zero vertical variation, but this would significantly increase the algebraic complexity. As an alternative, to more closely model a layer of finite depth, the system could be investigated for a small, but non-zero, fixed value of m, leading to a non-zero critical wavenumber and a non-zero critical parameter, K (see Figure 1). The solutions and stabilities of the resulting amplitude equation could then be determined. In particular, we would obtain a Ginzburg-Landau equation to describe temporal and spatial evolution of the solution amplitude (see Newell & Whitehead 1969; Chaté 1994). Next we investigate particular solutions to the first order equations. Namely, steady state and travelling solutions. The steady state solutions are described by a Hamiltonian system. These solutions are dependent on the function of integration,

K^*, which is itself dependent on z. The travelling solutions consist of horizontally drifting, long vertical plume solutions, and our analysis indicates that their speed is bounded within a very small range of values. Finally, we consider the second order non-linear partial differential equations and construct a solution that corresponds to vertically travelling pulses down regular plume structures. We derive an evolution equation for the general plume profile and calculate the speed of small amplitude pulses.

Biologically speaking, we analyse the mathematical structure of the governing equations and calculate that the easily-applied linear theory is adequate to predict the distance between the first plumes to appear in a well mixed deep suspension of *C. nivalis*. In other words, by fixing the dimensions of the container we can predict the distance between the very first plumes to occur just by analysing the accumulative behaviour of individual micro-organisms. We also calculate the profiles of well established plume solutions, which again can be compared directly with experimental measurements. Significantly, we investigate the occurrence of horizontally drifting plumes subject to a forcing flow field. We show that it is possible to predict the speed that these plumes will drift at and to calculate a cut-off value for the forcing, above which no drifting plume solutions exist. Both these aspects can be compared directly with experiments to help determine whether the full theory is consistent. Finally, we provide an analysis of the higher order equations and calculate solutions for pulses that can travel down long plume structures. These solutions can be used to provide a comparison with experimentally determined concentration or flow field profiles of the travelling pulses (frequently observed in deep suspensions) after a minor computation. The solutions described above and their comparison with experiments will form a basis from which to verify (or point towards problems with) the current theoretical understanding of the mechanisms involved in the phenomenon of bioconvection.

We would like to thank Dr. P. E. Hydon for many helpful suggestions. M.A.B. gratefully acknowledges the financial support of the EPSRC through an Earmarked award in Mathematical Biology.

11 Appendix

The definitions for the functions $A_j^i(\zeta)$ (from Bees *et al.* 1998b) are

$$\begin{aligned}
A_1^0(\zeta) &= \frac{825}{4\pi}\frac{5589+2420\zeta^2}{1098075\zeta^4+2363735\zeta^2+2772144} \\
A_1^1(\zeta) &= \frac{1815\zeta}{4\pi}\frac{1887+1210\zeta^2}{1098075\zeta^4+2363735\zeta^2+2772144} \\
A_2^0(\zeta) &= \frac{605}{8\pi}\frac{11178-4235\zeta^2}{1098075\zeta^4+2363735\zeta^2+2772144} \\
A_2^1(\zeta) &= \frac{2495625}{4\pi}\frac{\zeta}{1098075\zeta^4+2363735\zeta^2+2772144} \\
A_2^2(\zeta) &= \frac{1830125}{16\pi}\frac{\zeta^2}{1098075\zeta^4+2363735\zeta^2+2772144}.
\end{aligned} \tag{137}$$

Below are the definitions for the operators $\mathcal{A}_1(F)$ and $\mathcal{A}_2(F)$ used in Section 9:

$$\begin{aligned}
&\mathcal{A}_1(F) = \nabla^2\left((\mathbf{u}\cdot\nabla)\nabla_H^2 F\right) \\
&\equiv \left(\partial_x^2+\partial_y^2+\partial_z^2\right)\left(\partial_x\partial_z F\partial_x\nabla_H^2 F+\partial_y\partial_z F\partial_y\nabla_H^2 F-\nabla_H^2 F\partial_z\nabla_H^2 F\right)
\end{aligned} \tag{138}$$

and

$$\begin{aligned}
&\mathcal{A}_2(F) = \partial_z\nabla\cdot\left((\mathbf{u}\cdot\nabla)\,\mathbf{u}\right) \\
&\equiv \partial_z\partial_x\left(\partial_x\partial_z F\partial_x^2\partial_z F+\partial_y\partial_z F\partial_x\partial_y\partial_z F-\nabla_H^2 F\partial_z^2\partial_x F\right) \\
&+\partial_z\partial_y\left(\partial_x\partial_z F\partial_x\partial_y\partial_z F+\partial_y\partial_z F\partial_y^2\partial_z F-\nabla_H^2 F\partial_z^2\partial_y F\right) \\
&-\partial_z^2\left(\partial_x\partial_z F\partial_x\nabla_H^2 F+\partial_y\partial_z F\partial_y\nabla_H^2 F-\nabla_H^2 F\partial_z\nabla_H^2 F\right),
\end{aligned} \tag{139}$$

where

$$\mathbf{u} = \nabla\wedge\nabla\wedge(F\mathbf{k}). \tag{140}$$

References

[1] N. J. Balmforth. Solitary waves and homoclinic orbits. *Annual Review of Fluid Mechanics*, 27:335–373, 1995.

[2] M. A. Bees. *Non-Linear Pattern Generation in Suspensions of Swimming Micro-organisms.* PhD thesis, University of Leeds, 1996.

[3] M. A. Bees, P. Andresén, E. Mosekilde, and M. Giskov. The interaction of thin-film flow, bacterial swarming and cell differentiation in colonies of *Serratia liquefaciens*. *In preparation*, 1998a.

[4] M. A. Bees and N. A. Hill. Wavelengths of bioconvection patterns. *Journal of Experimental Biology*, 200:1515–1526, 1997.

[5] M. A. Bees and N. A. Hill. Linear bioconvection in a suspension of randomly swimming, gyrotactic micro-organisms. *Physics of Fluids*, 10(8):1864–1881, 1998.

[6] M. A. Bees, N. A. Hill, and T. J. Pedley. Analytical approximations for the orientation of small dipolar particles in steady shear flows. *Journal of Mathematical Biology*, 36:269–298, 1998.

[7] E. Buzano and M. Golubitsky. Bifurcation of the hexagonal lattice and the planar Bénard problem. *Philosophical Transactions of the Royal Society of LondonSeries A*, 308:617–667, 1983.

[8] C. J. Chapman and M. R. E. Proctor. Nonlinear Rayleigh-Bénard convection between poorly conducting boundaries. *Journal of Fluid Mechanics*, 101:759–782, 1980.

[9] H. Chaté. Spatiotemporal intermittency regimes of the one-dimensional complex Ginzburg-Landau equation. *Nonlinearity*, 7(1):185–204, 1994.

[10] S. Childress, M. Levandowsky, and E. A. Spiegel. Pattern formation in a suspension of swimming micro-organisms: equations and stability theory. *Journal of Fluid Mechanics*, 69:595–613, 1975.

[11] S. Childress and E. A. Spiegel. Pattern formation in a suspension of swimming microorganisms: Nonlinear aspects. Unpublished, 1978.

[12] P. Coullet and S. Fauve. *Collective modes of periodic structures, combustion and non-linear phenomena.* Les Editions de Physique, 1985.

[13] P. G. Drazin and W. H. Reid. *Hydrodynamic Stability.* Cambridge University Press, 1982.

[14] S. Fauve. GFD lecture notes. Technical report, Woods Hole Oceanographic Institute, Woods Hole, Massachussetts MA02543, 1985.

[15] M. Golubitsky, J. W. Swift, and E. Knobloch. Symmetries and pattern selection in Rayleigh-Bénard convection. *Physica D*, 10:249–276, 1984.

[16] N. A. Hill and D. P. Häder. A biased random walk model for the trajectories of swimming micro-organisms. *Journal of Theoretical Biology*, 186:503–526, 1997.

[17] N. A. Hill, T. J. Pedley, and J. O. Kessler. Growth of bioconvection patterns in a suspension of gyrotactic micro-organisms in a layer of finite depth. *Journal of Fluid Mechanics*, 208:509 – 543, 1989.

[18] E. L. Ince. *Integration of ordinary differential equations.* Oliver & Boyd, Edinburgh and London, seventh edition, 1956.

[19] M. S. Jones, L. le Baron, and T. J. Pedley. Biflagellate gyrotaxis in a shear flow. *Journal of Fluid Mechanics*, 281:137 – 158, 1994.

[20] J. O. Kessler. Gyrotactic buoyant convection and spontaneous pattern formation in algal cell cultures. In M. G. Velarde, editor, *Non-equilibrium cooperative phenomena in physics and related fields*, pages 241–248. New York: Plenum, 1984.

[21] J. O. Kessler. Hydrodynamic focussing of motile algal cells. *Nature*, 313:218–220, 1985a.

[22] J. O. Kessler. Co-operative and concentrative phenomena of swimming micro-organisms. *Contempory Physics*, 26(2):147–166, 1985b.

[23] E. Knobloch. Pattern selection in long-wavelength convection. *Physica D*, 41:450–479, 1990.

[24] A. C. Newell and J. A. Whitehead. Finite bandwidth, finite amplitude convection. *Journal of Fluid Mechanics*, 38:279–303, 1969.

[25] T. J. Pedley, N. A. Hill, and J. O. Kessler. The growth of bioconvection patterns in a uniform suspension of gyrotactic micro-organisms. *Journal of Fluid Mechanics*, 195:223 – 237, 1988.

[26] T. J. Pedley and J. O. Kessler. A new continuum model for suspensions of gyrotactic micro-organisms. *Journal of Fluid Mechanics*, 212:155 – 182, 1990.

[27] T. J. Pedley and J. O. Kessler. Hydrodynamic phenomena in suspensions of swimming micro-organisms. *Annual Review of Fluid Mechanics*, 24:313 – 358, 1992.

[28] A. Schlüter, D. Lortz, and F. Busse. On the stability of steady finite amplitude convection. *Journal of Fluid Mechanics*, 23:129–144, 1965.

[29] J. A. Whitehead. Fluid models of geological hotspots. *Annual Review of Fluid Mechanics*, 20:61–87, 1988.

Figure Captions:

Figure 1: Curves of marginal stability for a homogeneous suspension of large depth. Two cases are indicated. If $m = 0$ then the bifurcation is stationary and the growth rate is zero along the solid diagonal line and the line $k = 0$. If $m \neq 0$ then we have a Hopf bifurcation in which the real part of the linear growth rate is zero along the dotted line.

Figure 2: A plot of the linear growth rate for a mode with $m = 0$ and horizontal wavenumber k, for a value of the parameter K slightly above the critical value of 0. Here, $\mathrm{Re} = 10^{-3}$ and $K = 0.1$.

Figure 3: A selection of periodic orbits for $K^* = 0.1$ going clockwise with increasing x.

Figure 4: Profiles of the orbits given in Figure 3. Examples of N varying in the x direction for $K^* = 0.1$. Note how the wavelength increases with the maximum amplitude of the solution.

Figure 5: Nullclines (solid lines) for a typical travelling wave system where $c+E(p_0) \leq 0$. The arrows indicate the direction of the flow and the long-dashed lines indicate the manifolds of the saddle point, B. B allows the possibility of a homoclinic orbit around the focus, A, and as the focus, A, changes stability a limit cycle can develop. This ensures the existence of a Hopf bifurcation. The equilibrium point C is not within the region of realistic cell concentrations.

Figure 6: Travelling wave solutions exist for a small range of wavespeeds, c, for given values of the parameters Re, K^* and p_0. Here $K^* = 0.1$, $\mathrm{Re} = 0.4$ and p_0 is plotted along the x axis. The hatched region indicates where travelling wave solutions exist. Here, the value of Re is artificially large so that

the hatched region can be clearly seen. Normally Re $\sim 10^{-4}$ and the region is much smaller.

Figure 7: Spiral trajectories for the travelling wave system (clockwise with Ξ) where an unstable limit cycle can be clearly observed. $K^* = 0.1$, $p_0 = 0.4$, Re $= 0.4$ and $c = 0.15$.

Figure 8: Cell concentration for a horizontally travelling plume solution, varying with $x - ct$ for waves travelling to the right. In this example, each peak indicates a high local cell concentration and, therefore, a plume extended in the vertical direction. $K^* = 0.1$, $p_0 = 0.4$, Re $= 0.4$ and $c = 0.15$.

Figure 9: A plot of the perturbation, p_1 (solid line), to p_0 (dotted line) varying with x for a vertically travelling pulse down a plume. The perturbation indicates the form of the vorticity deviation to the regular plume solution. Here $K^* = 0.01$ with the initial conditions $n_0 = 5$, $p_0 = 0$, $n_1 = 13.8$ and $p_1 = 0$.

Figure 10: Perturbation, n_1 (solid line), to the cell concentration, n_0 (dotted line), varying with x for a vertically travelling pulse. The perturbation indicates the small amplitude variation in the vertical direction of the regular cell concentration profile. Adding small positive or negative values of n_1 to n_0 results in either a more sharply peaked distribution or a fatter plume respectively. Here $K^* = 0.01$ with the initial conditions $n_0 = 5$, $p_0 = 0$, $n_1 = 13.8$ and $p_1 = 0$.

parameter name	expression	typical value
λ	$1/2BD_r$	2.2
$\mathcal{N}$	$\langle V^2\rangle/V_s^2$	1.3
CASE 1: $\tau = 1.3$s and $B = 3.4$s		
Re	$\tau V_s^2\rho/\mu$	5.2×10^{-5}
Ri	$n_0 v\Delta\rho g\tau/\rho V_s$	$5.2\times10^{-6}\bar{n}$
η	B/τ	2.6
CASE 2: $\tau = 5$s and $B = 6.3$s		
Re	$\tau V_s^2\rho/\mu$	2×10^{-4}
Ri	$n_0 v\Delta\rho g\tau/\rho V_s$	$2\times10^{-5}\bar{n}$
η	B/τ	1.3

Table 1: Key parameter expressions and estimates. Case I refers to original estimates of the parameters as suggested by Pedley & Kessler (1990) and Case II to alternative estimates (Bees & Hill 1998; Jones *et al.* 1994)

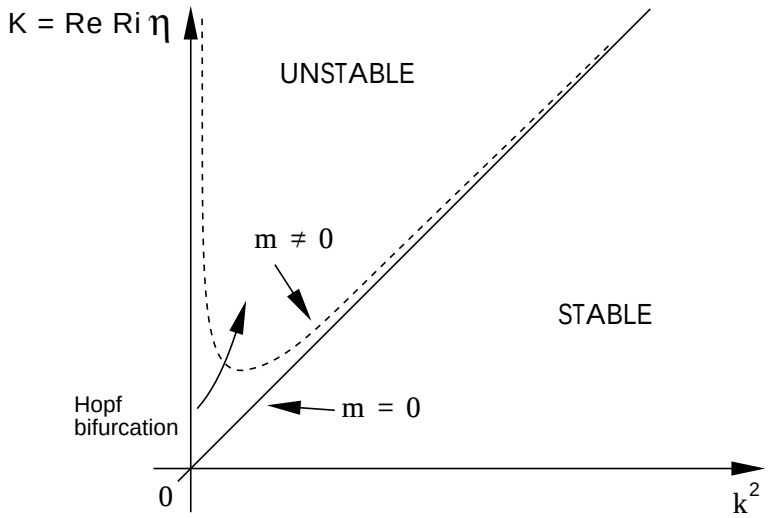

Figure 1:

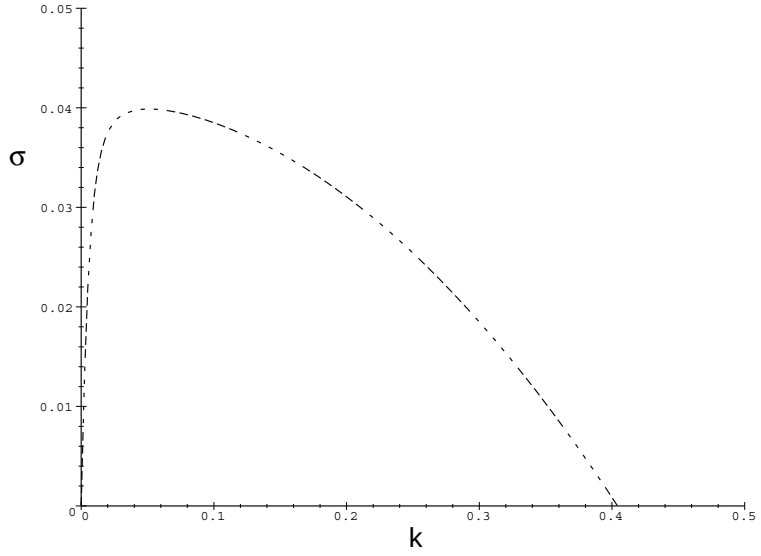

Figure 2:

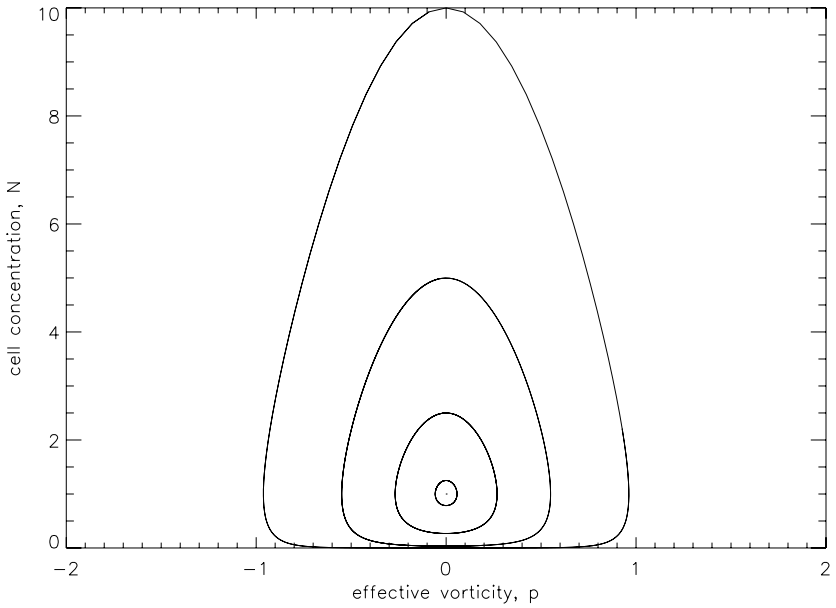

Figure 3:

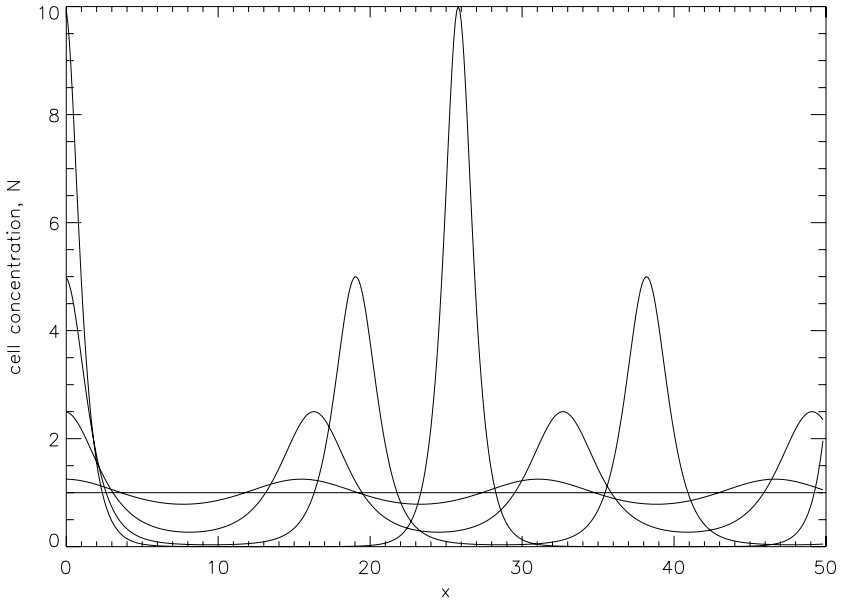

Figure 4:

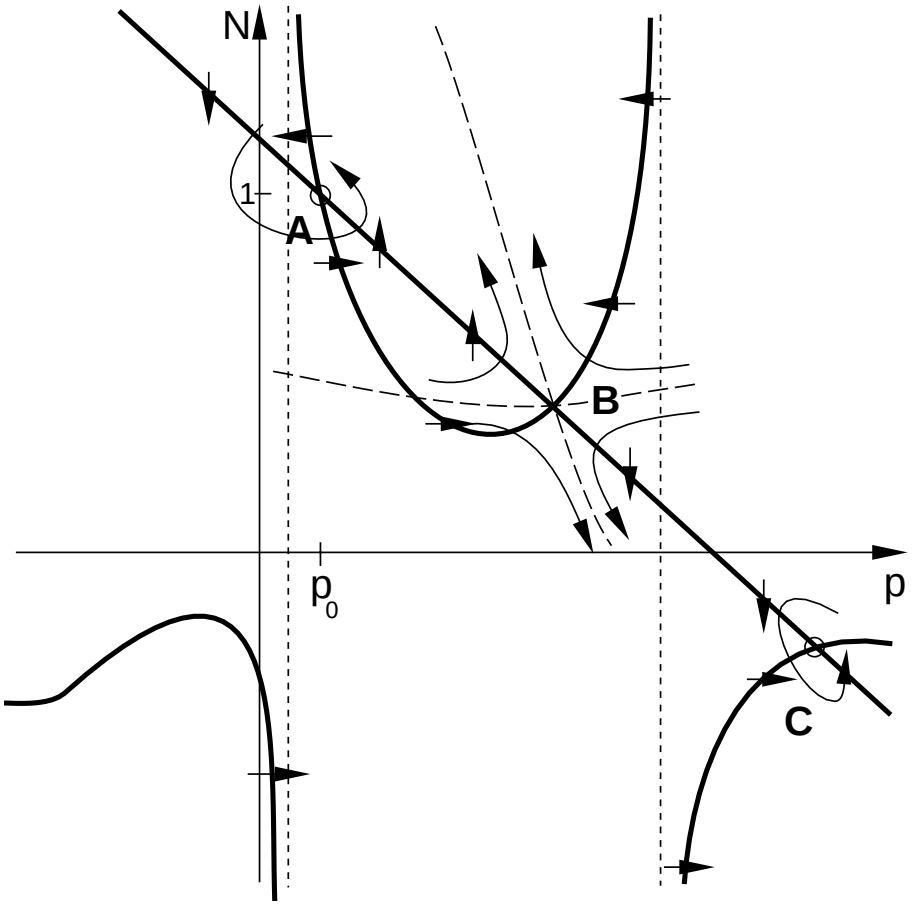

Figure 5:

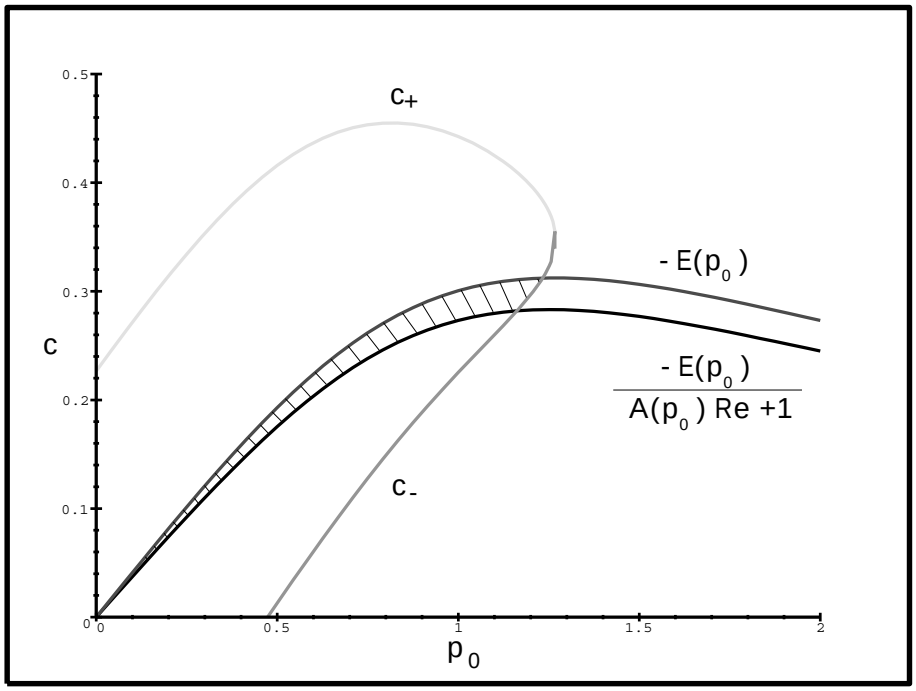

Figure 6:

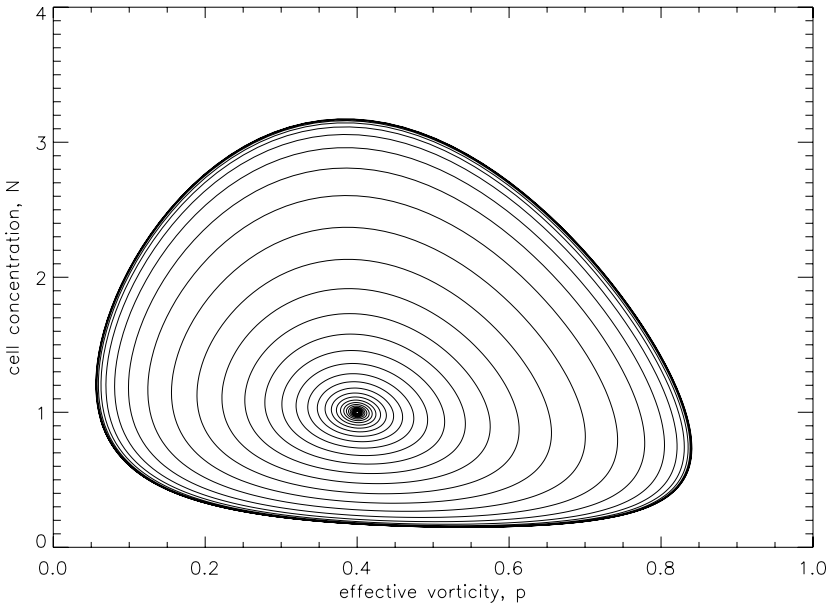

Figure 7:

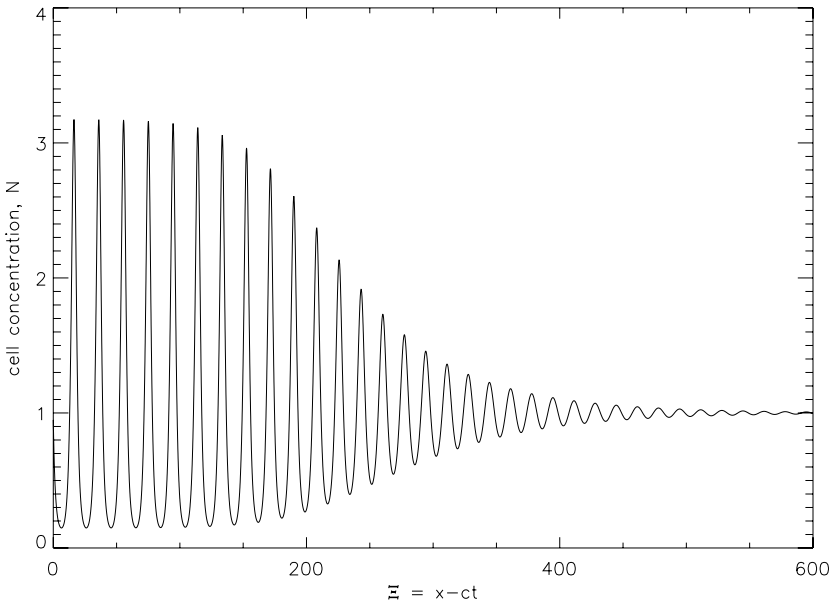

Figure 8:

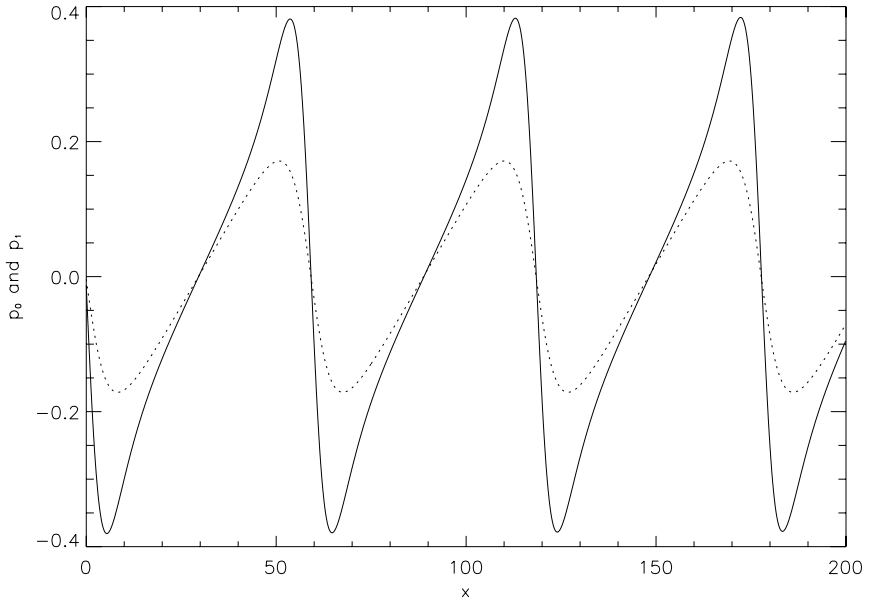

Figure 9:

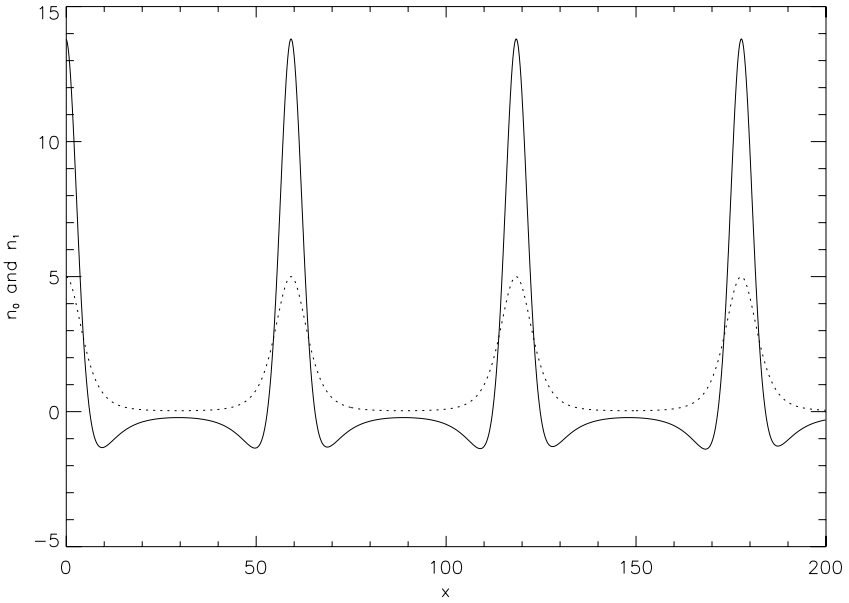

Figure 10: